New Photointermediates in the Two Photon Signaling Pathway of Sensory Rhodopsin-I†

Trevor E. Swartz,‡ Istvan Szundi,‡ John L. Spudich,§ and Roberto A. Bogomolni*,‡

Department of Chemistry and Biochemistry, University of California, Santa Cruz, California 95064, and Department of Microbiology and Molecular Genetics, University of Texas Medical School, Houston, Texas 77030

Received June 12, 2000; Revised Manuscript Received October 10, 2000

ABSTRACT: Sensory rhodopsin-I (SRI) functions as a color discriminating receptor in halobacterial phototaxis. SRI exists in the membrane as a molecular complex with a signal transducer protein. Excitation of its thermally stable form, SRI_{587}, generates a long-lived photointermediate of its photocycle, S_{373}, and an attractant phototactic response. S_{373} decays thermally in a few seconds into SRI_{587}. However, when S_{373} is excited by UV−blue light, it photoconverts into SRI_{587} in less than a second, generating a repellent phototactic response. Only one intermediate of this back-photoreaction, S^b_{510}, is known. We studied the back-photoreaction in both native SRI and its transducer free form fSRI by measuring laser flash induced absorption changes of S_{373} photoproducts from 100 ns to 1 s in the 350−750 nm range. Using global exponential fitting, we determined the spectra and kinetics of the photointermediates. S_{373} and fS_{373} when pumped with 355 nm laser light generate in less than 100 ns two intermediate species: a previously undetected species that absorbs maximally at about 410 nm, S^b_{410}, and the previously described S^b_{510}. These two intermediates appear to be in a rapid equilibrium, which probably entails protonation change of the Schiff base chromophore. At pH 6 this system relaxes to SRI_{587} via another intermediate absorbing maximally around 550 nm, which thermally decays back to the ground state. The same intermediates are seen in the presence and absence of transducer; however, the kinetics are affected by binding of the transducer.

The sensory rhodopsins (SRI and SRII) are photoreceptors that mediate phototactic responses in the archaeon *Halobacterium salinarum* (for reviews see refs *5* and *6*). This organism is motile, propelled by a polar flagellum. The cells perceive yellow-orange light as an attractant and UV−blue light as a repellent.

The sensory rhodopsins are integral membrane retinylidene chromoproteins highly homologous to the light-driven ion pumps bacteriorhodopsin, bR, and halorhodopsin, hR (reviewed in refs *5*−*7*). They contain seven membrane-spanning α-helical segments with an *all-trans* retinal bound to a lysine side chain via a protonated Schiff base linkage (*2*, *8*). In their native state, SRI and SRII [SRII is also known as phoborhodopsin or pR (*9*)] are complexed to dimers of their halobacterial transducer proteins HtrI and HtrII, respectively (*10*). These transducer proteins are approximately 60 kDa membrane spanning proteins homologous to bacterial chemotaxis receptor proteins (*11*, *12*). These transducer proteins modulate cytoplasmic enzymatic cascades (reviewed in ref *12*) that generate chemical signals, which control the direction of flagellar motor rotation (*5*).

SRII is active in the blue-green spectral range and mediates exclusively repellent signal responses (*9*, *13*−*15*). In contrast, sensory rhodopsin-I is a unique photoreceptor that mediates both attractant and repellent phototactic responses. Because of this dual function, SRI has been described as a color-discriminating light receptor (*16*). The ability to interpret color and intensity of light is a function of both the photoreceptor and the signaling complex with its associated signaling cascade. The photochemical properties of SRI and of one of its photochemical products are the key to this color-discriminating function.

In its ground state, SRI absorbs maximally at 587 nm (SRI_{587}); upon excitation by orange light, it proceeds through a photocycle $S_{610} \rightarrow S_{560} \rightarrow S_{373} \rightarrow SRI_{587}$ (*17*).[1] These intermediates are analogous to the K, L, and M intermediates in bR and have been referred to as SR^k, SR^L, and SR^M (*18*, *19*). S_{373} is the longest lived of the intermediates ($t_{1/2} = 800$ ms) (*17*), and on the basis of the effect of analogue chromophores that perturb the attractant response it has been concluded to be the signaling state because retinal analogues

† This work was supported by faculty research funds granted by the University of California, Santa Cruz (to R.A.B.), and by National Institutes of Health Grant R01-GM27750 (to J.L.S.).

* Corresponding author. Telephone: (831) 459-4294. Fax: (831) 459-2935. E-mail: bogo@chemistry.ucsc.edu.

‡ University of California, Santa Cruz.

§ University of Texas Medical School.

[1] The nomenclature used in this paper and proposed for further papers in this field is as follows. Photointermediates of each pigment are named using their bR-like intermediate notation. The nomenclature should be the pigment name with I, J, K, L, M, N, O, etc. as superscripts (or a superscript star, e.g., SRI*, to indicate an excited state) and their wavelengths of maximal absorbance as subscripts. This nomenclature is already in use for halorhodopsin (*1*−*3*). The SRI intermediates would be SRI^K_{610}, SRI^L_{560}, and so on. The same rule would be applicable to SRII and pSRII (pharaonis SRII) (*4*) intermediates. The only exception is S_{373}, which is a physiologically active photoreceptor that could be named both as an intermediate of the SRI photocycle and as another "sensory rhodopsin". We propose to maintain the nomenclature of the S_{373} back-reaction intermediates as S^b_λ, where λ is their wavelength of maximal absorbance. For transducer (Htr) free sensory rhodopsin samples, we prefix the notation with the letter f, for example, $fSRI^L_{560}$.

10.1021/bi0013290 CCC: $19.00
Published on Web 11/16/2000

proportionally increase the S_{373} lifetime and the attractant response of the cells (*20*). Excitation of S_{373} with UV−blue light results in recovery of the ground-state SRI_{587} via a path different from the thermal relaxation of S_{373}. Only one intermediate state of the S_{373} photoreaction (referred in this work as the back-reaction), S^b_{510}, has been previously identified (*8*, *16*, *21*). S_{373} contains an unprotonated, 13-*cis* retinal Schiff base (*8*, *22*), whereas the ground-state pigment contains an *all-trans* protonated chromophore. Reconversion of S_{373} into SRI_{587} requires at least two sequential steps: a photoisomerization followed by reprotonation of the aldimine. S^b_{510} has been tentatively assigned to contain an *all-trans* chromophore (*23*), and on the basis of S^b_{510}'s long-wavelength absorbance, the Schiff base linkage presumably is already protonated (*7*). Typically, the primary result of photoexcitation of retinal chromophores in rhodopsins is a subnanosecond reaction (*7*, *24*), with proton-transfer reactions and protein relaxation occurring at later times. This suggests that S^b_{510} cannot be the earliest species in the photoreaction and that there could be other intermediates capable of signaling HtrI to elicit the repellent response. Clearly, identification of the repellent signaling state and the signaling interactions between S_{373} and HtrI requires full characterization of the back-photoreaction.

Archaeal mutants that lack the gene for HtrI have been constructed to produce the photoreceptor SRI without its transducer protein (*26*). We refer to this transducer-free chromoprotein as fSRI (*25*). Proton binding equilibria, proton translocation reactions, and photoreactions of SRI are modified by the presence of SRI's transducer protein (*26*−*29*). Deprotonation of SRI_{587} at high pH induces a spectral shift to shorter wavelengths with an apparent p*K* around 8.5 (*30*), generating SRI_{552} (*31*). The p*K* for this transition is lowered to 7.2 in transducer-free SRI (*27*, *29*). This is a clear indication of the intimate interaction between SRI and its transducer protein. It has been shown that Asp76 is the group that changes protonation state in this transition (*27*) (Asp76 corresponds to Asp85 in bR). Asp76 is protonated in SRI_{587} but deprotonated in SRI_{552} (*32*). The most apparent difference between SRI and fSRI's photochemical behavior is the strong influence of the pH on the decay kinetics of fS_{373}. This reprotonation reaction is slowed in fS_{373} by about an order of magnitude in time per pH unit between pH 4 and pH 7.5 (*26*), whereas the decay of S_{373} is essentially constant in that pH range, suggesting that, in fSRI, Asp76 is either exposed to the medium or is accessible via proton-transferring side chains.

The two species, $fSRI_{587}$ and $fSRI_{552}$, have significantly different photoreactions, but both photocycles show similar lifetime dependence of fS_{373} on medium pH (*33*, *34*). However, $fSRI_{552}$ functions as a light-driven proton pump similar to bR (*29*, *35*), mainly because Asp76 is unprotonated and can serve as a proton acceptor (as Asp85 does in bR). However, Asp76 in SRI_{587} is protonated, therefore blocking the primary proton-transfer reaction of the pumping photocycle (*5*, *32*, *35*).

Despite their nearly identical spectral properties, $fSRI_{587}$ and native SRI_{587} have photocycle kinetic schemes that are significantly different, further emphasizing the close interaction between the photoreceptor and its transducer protein (*33*). However, it is not known whether the S_{373} photoreaction is also affected by the presence of HtrI.

The back-reaction of S_{373} has been only partially characterized, and the back-reaction of fS_{373} has not been studied. Understanding of this two photon reaction pathway is key to elucidation of the repellent signaling function of SRI. In addition, comparing the S_{373} and the fS_{373} photoreactions may provide additional insight into the interaction between the photoreceptor and its transducer. In this work we characterize the back-reactions of both SRI and fSRI in the 100 ns to 1 s time window and 350−750 nm spectral range and demonstrate the effects of HtrI on the kinetics of this reaction. Two new photointermediates are identified, which may be implicated in repellent signaling by the S_{373} photoreaction.

MATERIALS AND METHODS

Sample Preparation. Envelope vesicles containing fSRI and SRI were prepared as described elsewhere (*36*). Two samples were evaluated: one, which we call nativelike SRI envelope vesicles, contained overexpressed photoreceptor and its transducer protein. The second sample, fSRI envelope vesicles, was produced from a mutant strain that did not contain the gene for the transducer protein. The pH of the vesicle suspension in 4 M NaCl was adjusted by adding small amounts of HCl or NaOH. To study $fSRI_{587}$, the fSRI sample was measured at pH 6, where about 94% of the fSRI is in the $fSRI_{587}$ form. Envelope vesicles of nativelike SRI were measured at pH 7.

Time-Resolved Absorption Changes. Light-induced absorbance changes were measured in the 350−750 nm spectral range with a gated Optical Multichannel analyzer (OMA) (EG&G PAR) attached to a Jarrell-Ash monochromator (Monospec 27). Gate pulses of 10 ns duration were delivered by a high-voltage fast pulser (EG&G PAR Model 1302). Laser excitation pulses at 355 nm with a 10 ns pulse width were provided by the third harmonic of a pulsed Nd:Yag laser (Quanta-Ray Model DCR-1A). The "white" measuring pulse was provided by a microsecond Xe flash lamp (EG&G Model FX-800), powered by a high-voltage laboratory power supply (EG&G PAR Model PS-302). The samples were continuously pumped into the S_{373} or fS_{373} states by a red light provided by a 75 W xenon arc lamp, with a water heat filter (4 cm path length) and a high-pass optical filter that transmits light above 600 nm (Corning 2-62). The time delays between the probing beam and laser excitation pulse were arranged in a quasi-logarithmic time scale, at values of 1, 2, and 5 in each decade, and covered the time interval from 100 ns to 1 s. The spectral distribution of the measuring light was optimized by filters placed in the path of the probe beam. Synchronization of the OMA, gate pulse generator, Yag laser, and probe lamp was achieved by pulses delivered from a programmable pulse-delay generator (Stanford Research Systems Model DG535).

All absorbance measurements were carried out at room temperature (22 °C). The sample was placed in a quartz cuvette with a 5 mm path length. Actinic and probe beams entered the sample in a 90° geometry. All measurements were done at saturating laser intensities to avoid photoselection effects. Forty laser flashes at a frequency of 0.3 Hz were averaged for each time point. Care was taken to make sure the laser flashes were delivered after the system had fully relaxed from the previous pulse. The absorbance data were transferred to a PC computer for further analysis by

programs written in Matlab environment (The Math Works Inc., Natick, MA).

Low-Temperature, Light-Induced Absorption Changes. Low-temperature absorbance measurements were made on an Aminco DW-2 spectrophotometer computerized by Olis, Inc. (Bogart, GA), with an Aminco low-temperature attachment, using a 1 mm path length cell. The S_{373} and fS_{373} intermediates were trapped by cooling the sample to 77 K in the presence of red light >600 nm, provided by a filtered 75 W halogen light (Corning 2-62 filter). S_{373} and fS_{373} were illuminated at 77 K with light <400 nm by the same lamp (Corning 7-60 filter). S_{373} and fS_{373} photoproduct spectra were obtained from the difference between spectra taken before and after UV light irradiation of the respective samples.

Data Analysis. Absorption difference spectra taken at different time delays following the laser excitation pulse are arranged in the columns of a data matrix. Assuming that the dark reactions following the laser excitation are first-order processes, the data matrix can be represented by a sum of exponential functions. The exponents are called apparent rates, and the corresponding amplitudes are the b-spectra. Prior to the global exponential fit the data matrix is subject to singular value decomposition (SVD). Applying SVD to the data matrix (A) produces three new matrices (*37*):

$$A = USV' \quad (1)$$

where *U* contains the orthogonal basis spectra, *S* contains their significance values, and *V* contains the time dependence of the basis spectra. The *V* matrix is fit to a sum of exponentials, and finally the b-spectra are calculated (*37*). The basis spectra are linear combinations of the spectral forms of the intermediates (ϵ) present in the system and can be represented by the algebraic sum of the presumed intermediate spectra:

$$U = \epsilon Q \quad (2)$$

where *Q* is the composition matrix, whose elements represent the fractional contribution of each spectra (ϵ). The spectra of the intermediates included in the columns of the matrix (ϵ) are skewed Gaussians similar in shape to that of the ground-state SRI and other rhodopsin proteins previously described (*19*). The shape of the UV intermediate is taken from the light-induced difference spectrum of SRI (data not shown).

Substituting eq 2 into eq 1, the data matrix can be rewritten as

$$A = \epsilon QSV' \quad (3)$$

The data matrix (*A*) can also be represented as the product of the intermediate spectra (ϵ) and concentration (*C*) matrices.

$$A = \epsilon C \quad (4)$$

The time-dependent concentration of the individual spectral forms can be calculated from the composition matrix (*Q*) and the *S* and *V* matrices.

$$C = QSV' \quad (5)$$

A kinetic matrix, whose nondiagonal elements represent the microscopic rate constants, can then be fit to the *C* matrix. Each column of the kinetic matrix contains the microscopic rates of conversion of a particular intermediate into all of the others.

RESULTS

Under continuous red light, archaeal rhodopsins generate a photostationary state in which the concentration of thermal intermediates is determined by their respective rates of formation and decay. Because S_{373} has a very long decay time compared with all other thermal intermediates, it is the most abundant species in the stationary state. It has been shown that SRI can be fully converted into S_{373} at sufficiently high continuous red light intensities. A plot of the inverse ground-state absorbance bleach as a function of the inverse incident actinic light intensity for this system yields a straight line. This allows for an estimation of the total amount of initial pigment present in the sample by extrapolation to infinite actinic light intensity (*36*). We tested all of our samples using this approach to establish the actinic illumination conditions that would drive nearly all of the pigment into S_{373} or fS_{373}. At saturating UV laser excitation intensities, bleaching of S_{373} or fS_{373} did not exceed about 10% of the pigment, therefore perturbing only slightly the photostationary state. As the ground state regenerates in the back-reaction, it is reconverted into S_{373} by the constant red actinic light. This rate of reconversion is proportional to the light intensity and to the ground-state concentration. Too high a reconversion rate would complicate the interpretation of the kinetics of the last back-reaction step, which occurs in the 1 s time range. Therefore, we adjusted the actinic light to be high enough to bleach most of the ground state but limited its intensity to allow measurement of absorbance changes caused by the late intermediates of the back-reaction.

Photocycle of fS_{373}. The absorbance difference spectra measured at delays from 100 ns to 20 ms are represented in Figure 1A. After the formation of the earliest recorded photoproducts, no further thermal reactions occur for the first 20 ms. All of the thermal reactions that we detect occur in the 50 ms to 1 s time interval, as shown in Figure 1B. The data were smoothed by point averaging three consecutive points on the wavelength scale, which reduced the data set from 678 to 226 wavelengths. The kinetic data matrix was subjected to SVD, followed by global multiexponential fitting and kinetic modeling as described in Materials and Methods. An adequate exponential fit of the data was achieved by using two exponentials. The residual error decreases almost 30% in going from one to two exponentials. Both two and three exponential fittings give very low residual noise (Figure 2). Fitting to three exponentials gives an additional time constant in the microsecond range; however, the b-spectrum associated with this time constant is very small within our system noise, so we cannot justify using it in the analysis. We therefore resolve only two time constants at 70 ms and 2.9 s. Both the 2.9 s time constant and the corresponding b-spectrum are less reliable than the first apparent time constant and b-spectrum because they were obtained using information limited by our 1 s time window. In addition, the spectral changes of the reconversion of $fSRI_{587}$ to fS_{373} by the continuous red light and the thermal decay of fS_{373} into $fSRI_{587}$ contribute to the shape of the second b-spectrum. Therefore, the second b-spectrum provides only kinetic

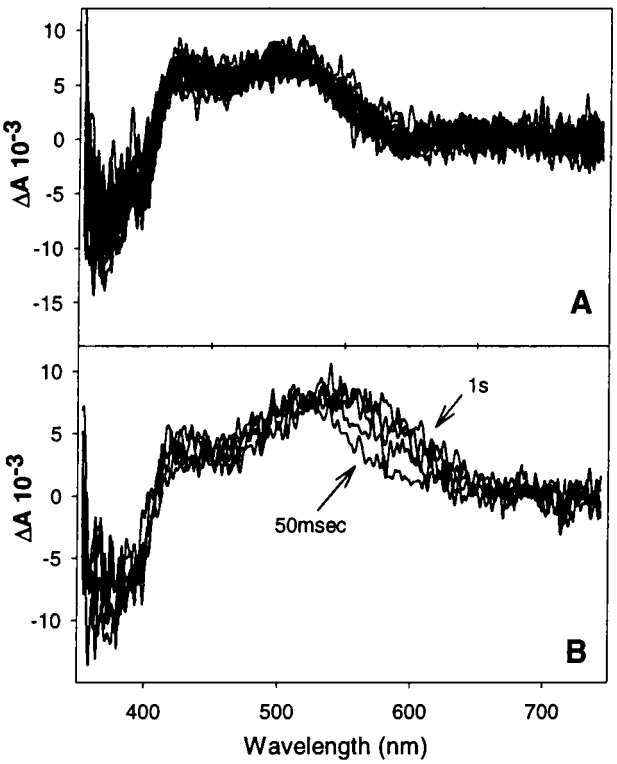

FIGURE 1: Difference absorption spectra of fSRI after excitation with a 355 nm laser pulse while under illumination with continuous red light. (A) Spectra collected between 100 ns and 20 ms after laser pulse. (B) Spectra collected between 50 ms and 1 s after laser pulse.

information and was not used in the numerical calculation of the microscopic rates in the kinetic matrix.

Our strategy in the derivation of the kinetic scheme is the following. First, we obtain the spectra of the proposed intermediates from the spectral decomposition of the first b-spectrum and the *U* vectors from SVD. Second, we calculate the time-dependent concentration of the intermediates from the results of SVD as described in Materials and Methods. Third, the concentration time dependence is fit to a kinetic scheme by adjusting the microscopic rates in the kinetic matrix until it reproduces the concentration time profile (see below). The scheme should also be consistent with the apparent rates and b-spectra of the global exponential fit.

(A) Spectra of Intermediates. We determined the spectral species (ϵ matrix) involved in the kinetic scheme by fitting spectral intermediates to the first b-spectrum and the first two *U* vectors. The intermediate species used in the fitting are shown in Figure 3. The first b-spectrum is fit by a linear combination of three intermediate spectra (criteria for the intermediate spectral shapes are discussed in Materials and Methods) plus the ground-state (SRI_{587}) spectrum (Figure 4). A ground-state spectrum contribution was required to satisfactorily fit the first b-spectrum. The required intermediates are as follows: one absorbs maximally at about 410 nm (we denote this species as fS^b_{410}); the second species resembles an intermediate previously described in SRI and absorbs maximally at 510 nm (fS^b_{510}) (*8*, *16*, *21*); the third intermediate absorbs maximally at 550 nm (fS^b_{550}). Note that the fS^b_{410} and fS^b_{510} species are present in the first b-spectrum in the same ratio as they are seen in the experimental difference spectra at early times. Therefore, these intermediates are combined into a single form representing an unresolved fast equilibrium mixture of the two intermediates, and the spectrum of this mixed form is also shown in Figure 3.

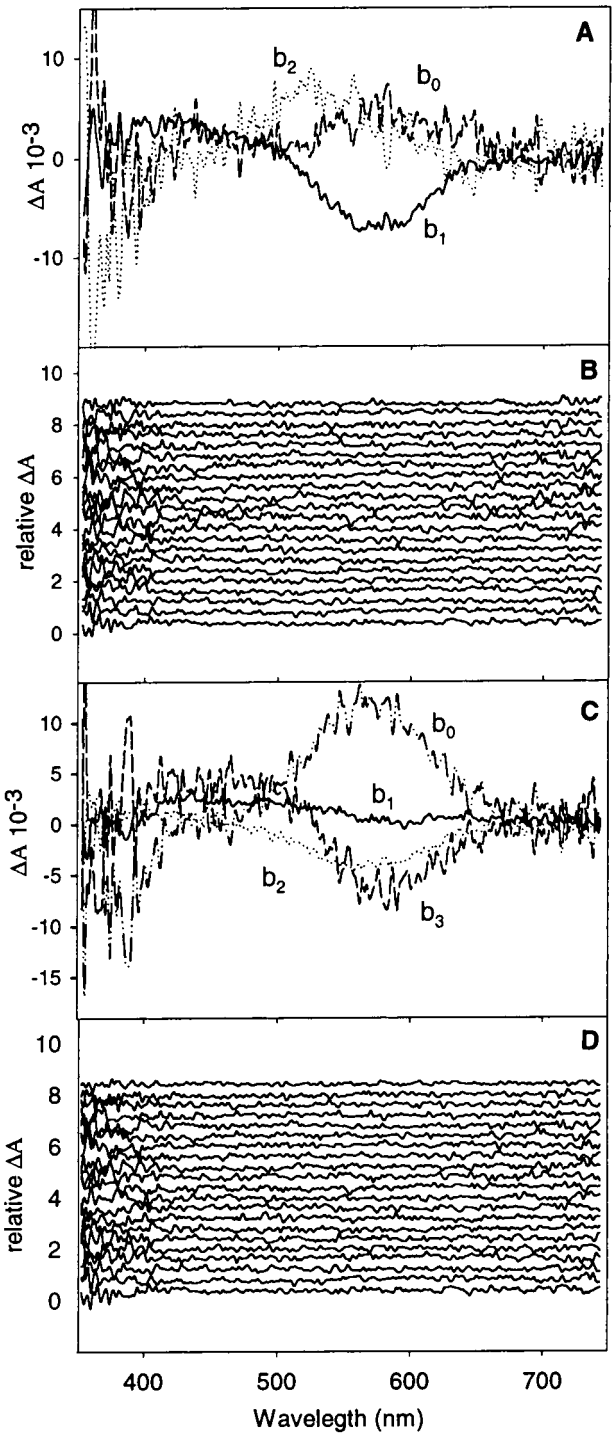

FIGURE 2: Results of global multiexponential fitting of difference absorption spectra from fSRI. (A) b-spectra with apparent rates of 70 ms and 2.9 s. (B) Residuals (difference between the data and least-squares fit). (C) Global exponential fitting to three exponentials. (D) Residuals for three exponential fitting.

(B) Time-Dependent Concentration of Intermediates. The first two *U* vectors fit satisfactorily (see Figure 5) with the linear combination of these intermediates, further supporting our choice intermediate spectra. Note that in the decomposition of the *U* vectors into intermediate spectra we used the combined spectrum of the fS^b_{410}/fS^b_{510} intermediates. From the decomposition of the *U* vectors we obtained a composi-

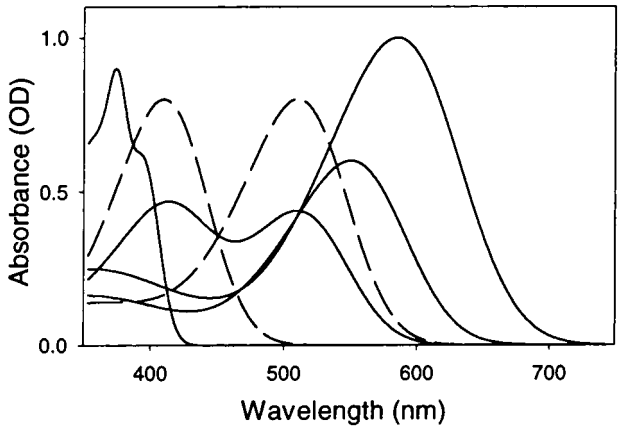

FIGURE 3: Spectral shapes of intermediates and the ground-state species used in data analysis. The fS^b_{410}/fS^b_{510} equilibrium species is the addition of fS^b_{410} and fS^b_{510} (dotted line).

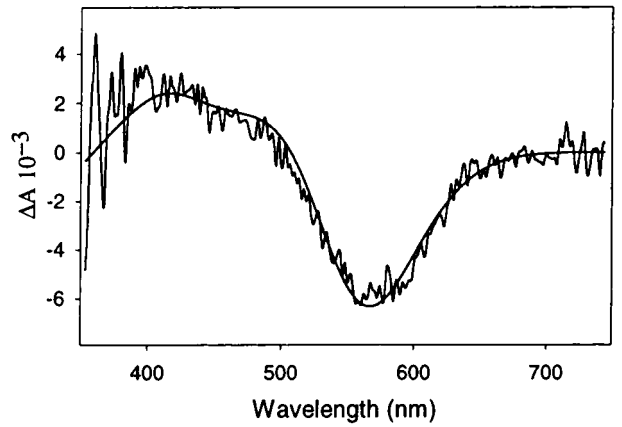

FIGURE 4: First b-spectrum of fSRI from the global multiexponential fit (70 ms apparent lifetime). The b-spectrum is fit with a linear combination of intermediates fS_{373}, fS^b_{410}/fS^b_{510}, fS^b_{550}, and the ground-state $fSRI_{587}$. The spectral shapes are shown in Figure 3.

tion matrix, which was combined with the *S* and *V* matrices to yield the time dependence of the intermediate concentrations as described in the Data Analysis section. The term concentration refers to the concentration change induced by the laser flash and will be used in this sense throughout the paper. The intermediates formed have a positive value, and the bleached fS_{373} form has a negative one. The algebraic sum of the concentrations was close to zero in the measurement time window, and as expected the concentration of the bleached fS_{373} form stayed nearly constant up to 100 ms, which indicates the consistency of the spectral decomposition (Figure 6).

(C) Kinetic Scheme. In proposing a kinetic scheme we rely mainly on the information contained in the first b-spectrum, which is not affected by the complications at late times. When the apparent rates are well separated, as in our case, the b-spectra can be interpreted as follows: intermediates that decay have positive amplitudes, and intermediates that are formed have negative amplitudes in the b-spectra. The fS^b_{410} and fS^b_{510} intermediates are in an unresolved fast equilibrium, as already mentioned, and decay simultaneously to fS^b_{550} and the ground-state form SRI_{587}. Because of this, we treated the fS^b_{410}/fS^b_{510} equilibrium as a single species whose spectrum is the sum of the fS^b_{410} and fS^b_{510} intermediates. The presence of fS^b_{550} and $fSRI_{587}$ in the first b-spectrum

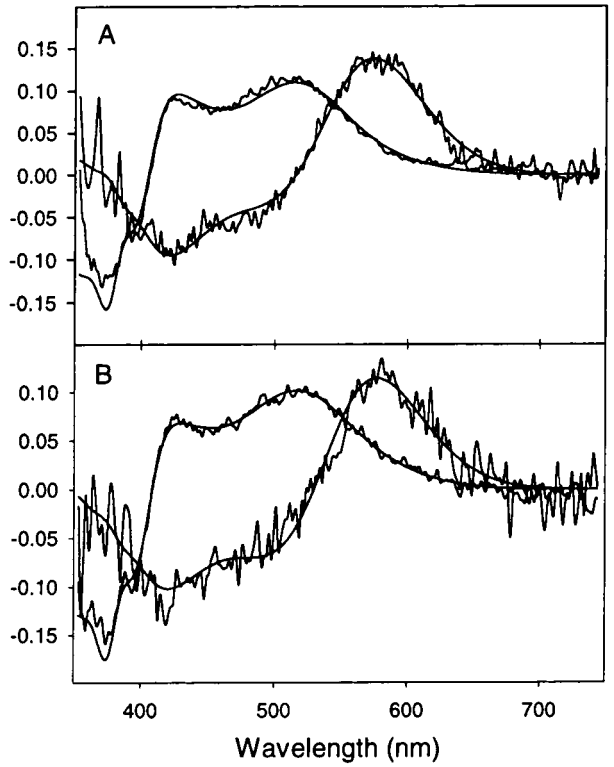

FIGURE 5: First two U vectors fit with a linear combination of intermediate fS_{373}, fS^b_{410}/fS^b_{510}, and fS^b_{550} spectra. (A) U vectors from fSRI. (B) U vectors from SRI.

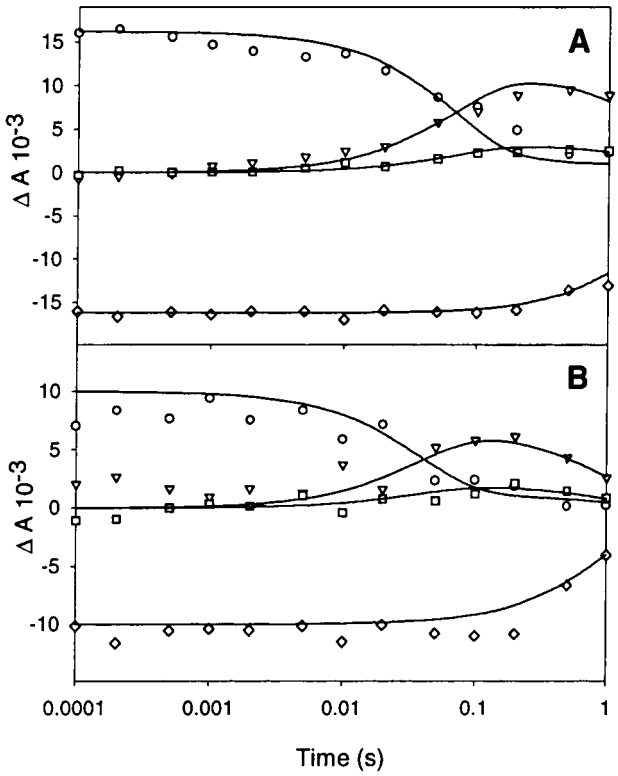

FIGURE 6: Concentration time-dependent profiles for intermediates. Solid lines are reproduced profiles using rate constants as described in the text. Symbols are intermediates represented in the C matrix, which represents the concentration of each intermediate present in the data: (○) $fS^b_{410/510}$, (▽) fS^b_{550}, (◇) fS_{373}, and (□) $fSRI_{587}$. (A) fSRI. (B) SRI.

with negative amplitudes indicates that the fS^b_{410}/fS^b_{510} species simultaneously generates fS^b_{550} and partially recon-

Scheme 1[a]

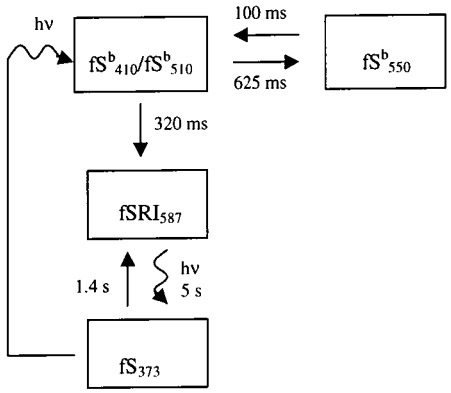

[a] fS$^b_{410}$/fS$^b_{510}$ is fS$^b_{410}$ + BH$^+$ ⇔ fS$^b_{510}$ + B$^-$. fS$^b_{410}$ contains an *all-trans* unprotonated Schiff base. fS$^b_{510}$ contains an *all-trans* protonated Schiff base.

verts to the ground state. This eliminates a sequential model in which fS$^b_{550}$ is an intermediate state between fS$^b_{410}$/fS$^b_{510}$ and the ground state. The most plausible explanation for the first b-spectrum is the existence of a branch as shown in Scheme 1. In this scheme the fS$^b_{410}$/fS$^b_{510}$ mixed species is shown in equilibrium with the fS$^b_{550}$ intermediate. The reversible step was introduced because the amplitude of the fS$^b_{410}$/fS$^b_{510}$ intermediate species in the first b-spectrum is less than the amount of fS$^b_{410}$/fS$^b_{510}$ present in the experimental difference spectra at early times. In a reversible transition one expects only a partial conversion of the fS$^b_{410}$/fS$^b_{510}$ mixed form to the fS$^b_{550}$ form. The conversion of the fS$^b_{410}$/fS$^b_{510}$ mixed form to the unphotolyzed form is not reversible. The additional two steps in the scheme reestablish the fS$_{587}$/ fS$_{373}$ photostationary state perturbed by the laser flash.

The kinetic matrix corresponding to Scheme 1 was fit to the concentration time dependence to determine the microscopic rate constants. It is assumed that all of the photolyzed S$_{373}$ is converted into an equilibrium mixture of fS$^b_{420}$/fS$^b_{510}$ at our fastest measurement time, 100 ns, and the fS$_{587}$/ fS$_{373}$ photostationary state is perturbed by the laser flash, resulting in an instantaneous depletion of the fS$_{373}$ concentration at the start of the reaction cascade. Note that in the description of the kinetics the concentrations of the fS$^b_{420}$/fS$^b_{510}$ and fS$^b_{550}$ intermediates are represented by their absolute values, while those of the fS$_{373}$ and fS$_{587}$ forms are represented by the differences from their steady-state values prior to laser photolysis. The microscopic rates were forced to reproduce the first apparent rate but not the second one. The rates for the establishment of the steady state by the continuous red light illumination are in accord with the values determined independently from single-wavelength experiments. The microscopic rate constants shown in the scheme reproduce the concentration time profile satisfactorily, as seen in Figure 6. In addition, using these microscopic rates and the spectra of the intermediates (ϵ), we reproduced the experimental data matrix within the measurement noise (Figure 7).

S$_{373}$ Photocycle. The data collected on the SRI sample (not shown) follows very closely that of the fSRI sample (Figure 1). However, the SRI data had a smaller signal-to-noise ratio than the fSRI sample because of the lower pigment contents of the SRI samples. Analysis of the SRI data followed identically that of fSRI. SVD and global exponential fitting

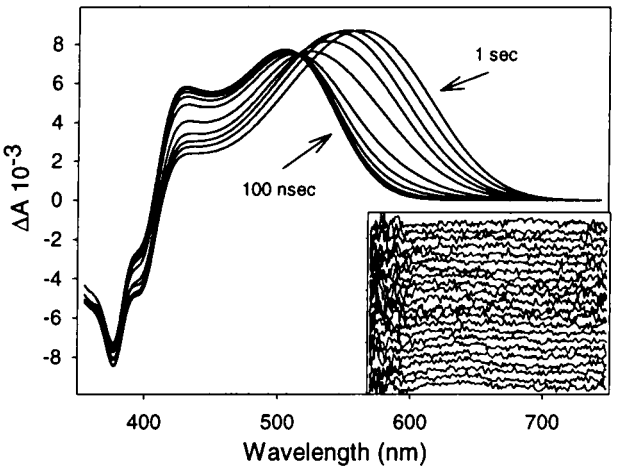

FIGURE 7: Reproduced data for fSRI using microscopic rates shown in Scheme 1 and spectral intermediates in Figure 3. Residuals of difference between data and reproduced data are shown in the inset.

Scheme 2[a]

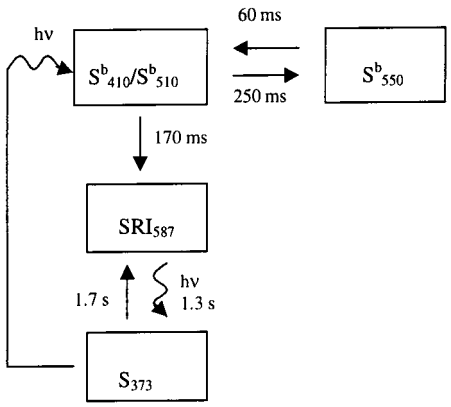

[a] S$^b_{410}$/S$^b_{510}$ is S$^b_{410}$ + BH$^+$ ⇔ S$^b_{510}$ + B$^-$. S$^b_{410}$ contains an *all-trans* unprotonated Schiff base. S$^b_{510}$ contains an *all-trans* protonated Schiff base.

of the SRI data gave two apparent lifetimes of 40 ms and 1 s. As was the case with fSRI, the later b-spectrum was complicated with multiple processes that did not go to completion during our measurement time window and therefore were not considered reliable. Fitting the b-spectrum associated with the 40 ms apparent lifetime required the same spectral intermediates as fSRI, with the inclusion of the ground-state SRI$_{587}$. The fitting of the *U* vectors to the intermediate spectra (Figure 5B) produced a composition matrix from which the time dependence of the intermediate concentrations was calculated, which was fitted by a kinetic scheme similar to the one found for fSRI (Figure 6B). The microscopic rates for the fit of the back-reaction of SRI are shown in Scheme 2. In this scheme, for HtrI complexed SRI we identify two new intermediate species, S$^b_{410}$ and S$^b_{550}$, which were not reported earlier. Intermediate S$^b_{410}$ is in an unresolved equilibrium with the previously identified intermediate S$^b_{510}$.

Low-Temperature Experiments. Further proof of the existence of the fS$^b_{410}$ and S$^b_{410}$ intermediates came from trapping this intermediate at liquid nitrogen temperatures, as shown in Figure 8. In both cases, it is possible to fit the low-temperature spectra as the algebraic sum of a bleached fSR$_{373}$ and a slightly red-shifted 410 nm species [this red shift at low temperature is typical of most retinal pigments (*39*)].

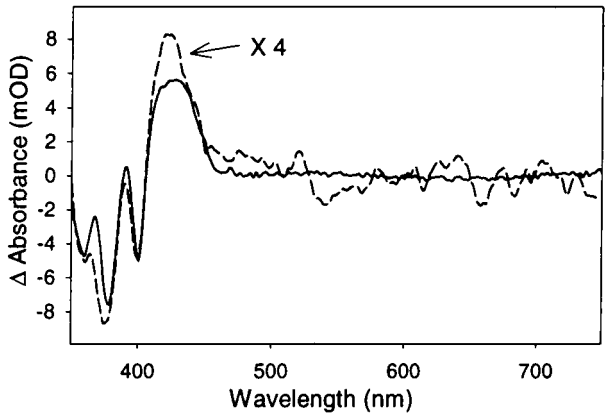

FIGURE 8: Light-induced absorption difference spectra produced at 77 K. The solid line is fSRI, and the dashed line is SRI.

DISCUSSION

Because of the similarities in the results of the fSRI and SRI back-reactions, the discussion of the protein and chromophore states applies to both of them. Our molecular model of the back-photoreactions of SRI is shown in Figure 9. The 410 nm state is trapped at 77 K, and from studies of other rhodopsins we expect only the primary chromophore isomerization process to occur at this low temperature (*40*, *41*); that is, the major protein changes are frozen. Most chromophore changes and intramolecular proton transfers are thermally activated and show very high activation energies in general. Because of this, we conclude that the primary light reaction is a *cis* to *all-trans* isomerization of the retinal (recall that fS_{373} is 13-*cis*), and the S^b_{410} species that we trap must contain therefore an *all-trans* retinal with an unprotonated Schiff base (*7*). The 410 nm absorption maximum of S^b_{410} is close to that observed in other *all-trans* unprotonated Schiff bases of archaeal rhodopsins. Halorhodopsin, hR_{578}, which contains an *all-trans* protonated chromophore (*2*), generates an *all-trans* unprotonated species in the dark (p*K* ~10), hR_{410} (*7*, *42*). In hR the protein residue structurally equivalent to bR's Asp85 is a threonine. Substituting a threonine or an asparagine residue in bR removes the native negative charge of aspartate 85, significantly lowering the p*K* of its Schiff base. Titration in the dark of these mutants generates at high pH a 410 nm absorbing species that contains an unprotonated *all-trans* chromophore (*43*−*45*). This is also a property of purified fSRI, which in its 587 nm form has a protonated Asp76 residue (corre-

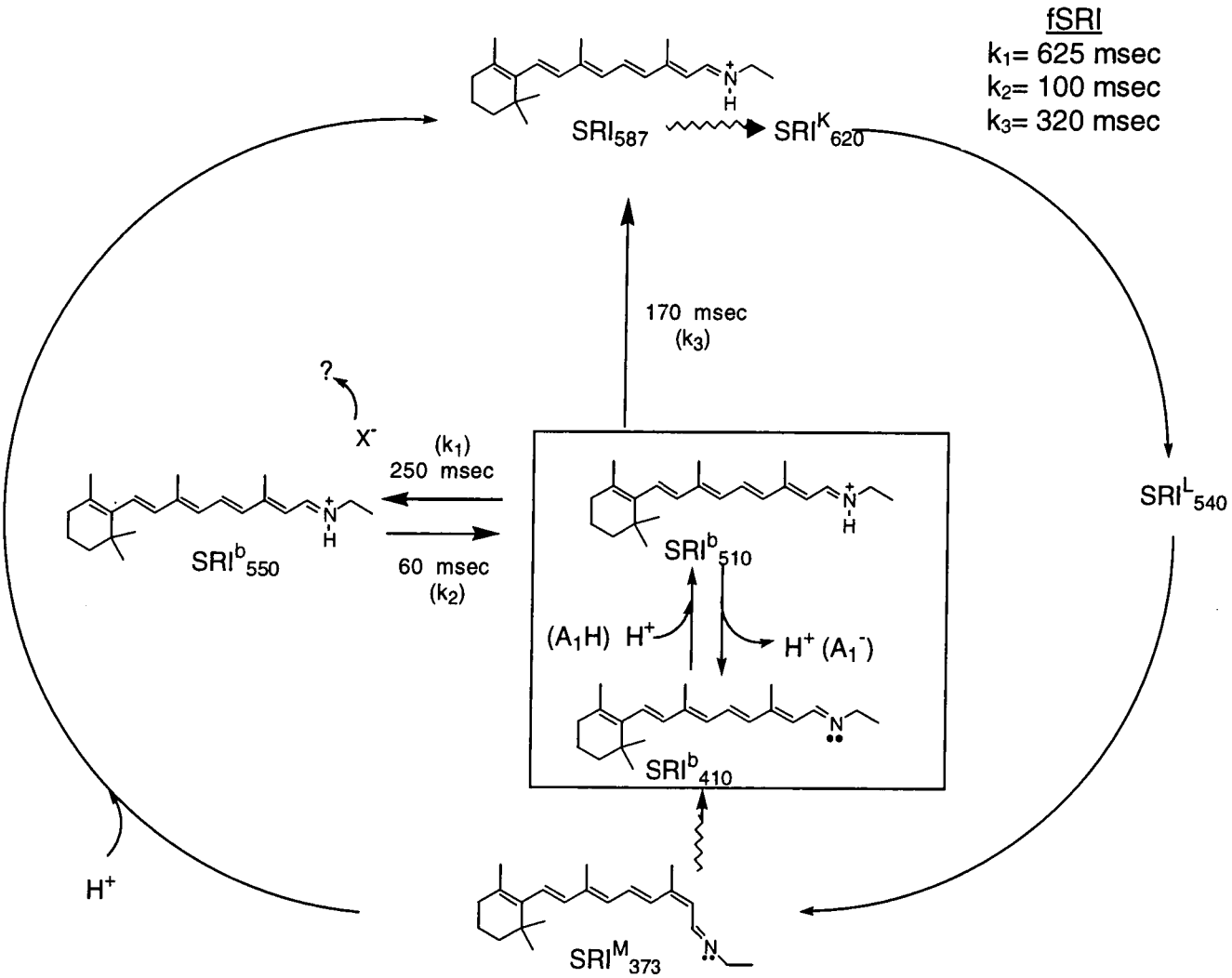

FIGURE 9: Model of back-photoreactions of SRI. X, A_1, and A_1 are protein residues involved in the proton exchange reactions proposed. We represent them as different groups, but they could be the same residue (for further details, see text). Kinetics for back-photoreactions of fSRI are shown in the top right of the figure.

sponding to Asp85 in bR). Purified SRI_{587} forms by deprotonation in the dark (titration pK ~6.5) a 400 nm species that contains presumably an *all-trans* chromophore, since no light reaction is involved in the transition (*46*). It appears that, in archaeal rhodopsins, an absorption maximum around 410 nm under conditions that remove the neighboring negative charge of their structurally equivalent aspartate (in SRI) residues indicates the presence of an unprotonated chromophore. We therefore tentatively assign the conversion of S^b_{410} to the intermediate S^b_{510} to be a protonation of the Schiff base nitrogen to produce a protonated *all-trans* Schiff base chromophore. At room temperature and at the fastest time we measure (100 ns), the equilibrium between these intermediates has already been established. If this equilibrium indeed represents a reversible proton-transfer reaction, it should be dependent on the medium pH if the chromophore is accessible from the aqueous phase. We observed that the back-reaction slows down at higher pH. However, the fS^b_{410}/fS^b_{510} equilibrium still develops at higher pH, but its decay is retarded. This is consistent with a model in which the formation of S^b_{510} involves a rapid proton-transfer reaction from a neighboring protonated protein residue followed by a rate-limiting reprotonation step. This interpretation would indicate that our earliest measuring time of 100 ns is sufficient for both an isomerization of the retinal and a proton-transfer reaction to occur. We speculate that the group that donated the proton, now negatively charged, probably moves away from the chromophore, further red shifting the absorption, resulting in the formation of the fS^b_{550} intermediate. At high pH, the ground state of fSRI shifts from $fSRI_{587}$ to $fSRI_{552}$. It has been shown that this shift is due to the deprotonation of Asp76 (*32*). Whether the group involved in these proton-transfer reactions that generate S^b_{510}, fS^b_{550}, and $fSRI_{587}$ is also Asp76 is unknown. However, it is an intriguing possibility because the transition $fS^b_{550} \rightarrow fSRI_{587}$ parallels closely the spectral transition $fSRI_{552} \rightarrow fSRI_{587}$, where the main event is a reprotonation of aspartate 76.

A plausible reaction sequence could be the following: (1) a proton is transferred reversibly from a neighboring donor group, generating the S^b_{410} /S^b_{510} proton equilibrium; (2) a slow protein relaxation (≈70 ms) perhaps increases the distance from the Schiff base to the negative charge of such donor group, creating a large barrier for the proton-transfer reaction from the chromophore to this group and causing the expected shift to longer wavelengths when a protonated retinal−Schiff base is distanced from its counterion ($fS^b_{510} \rightarrow fSR^b_{550}$); and (3) a final reprotonation of this residue from the medium that removes completely this negative charge with the predictable further shift to longer wavelengths as observed both in the $fS^b_{550} \rightarrow fSR_{587}$ and in the $fSR_{552} \rightarrow fSR_{587}$ transitions.

The intriguing question that motivated this study was identification of the signaling state in SRI that HtrI interprets as the presence of UV−blue light. It has been proposed that the longest lived thermal intermediate S_{373} is the signaling state for yellow light (*20*) and S^b_{510} was the only candidate for the back-reaction. However, we have now identified two new intermediates in the photocycle: S^b_{410} and S^b_{550}. Implicating either of these states as signaling states would be pure conjecture at this time. It is also an intriguing possibility that perhaps the protonation reaction $S^b_{410} + H^+ \rightarrow S^b_{510}$ could initiate a molecular conformation change in HtrI if the proton is donated by the transducer protein or, alternatively, if the SRI protein residue undergoing deprotonation interacts electrostatically with one or more groups of HtrI.

Interestingly, we also demonstrate that the recovery of the unphotolyzed state after absorption of UV−blue light by S_{373} is much slower than previously thought. This is because previous measurements were made with a single-wavelength instrument and did not allow for the discrimination between S^b_{550} and the ground-state SRI_{587}. This slower recovery of the unphotolyzed state means that, under steady-state conditions produced by illumination of "white light", a mixture of intermediate species could be present, depending on the relative intensities of the various wavelengths of light. To clarify physiologically important responses, further studies characterizing the swimming behavior of these organisms in various light environments, along with the associated photocycle of these pigments under the same light conditions, will be needed.

ACKNOWLEDGMENT

We thank Elena Spudich for very helpful discussion.

REFERENCES

1. Zimányi, L., and Lanyi, J. K. (1987) *Biophys. J. 52*, 1007−1013.
2. Fodor, S. P., Gebhard, R., Lugtenburg, J., Bogomolni, R. A., and Mathies, R. A. (1989) *J. Biol. Chem. 264*, 18280−18283.
3. Diller, R., Stockburger, M., Oesterhelt, D., and Tittor, J. (1987) *217*, 297−304.
4. Chizhov, I., Schmies, G., Seidel, R., Sydor, J. R., Luettenberg, B., and Engelhard, M. (1998) *Biophys. J. 75*, 999−1009.
5. Hoff, W. D., Jung, K. H., and Spudich, J. L. (1997) *Annu. Rev. Biophys. Biomol. Struct. 26*, 223−258.
6. Oesterhelt, D. (1998) *Curr. Opin. Struct. Biol. 8*, 489−500.
7. Haupts, U., Tittor, J., Bamberg, E., and Oesterhelt, D. (1997) *Biochemistry 36*, 2−7.
8. Tsuda, M., Nelson, B., Chang, C. H., Govindjee, R., and Ebrey, T. G. (1985) *Biophys. J. 47*, 721−724.
9. Tomioka, H., Takahashi, T., Kamo, N., and Kobatake, Y. (1986) *Biochem. Biophys. Res. Commun. 139*, 389−395.
10. Zhang, X. N., and Spudich, J. L. (1998) *J. Biol. Chem. 273*, 19722−19728.
11. Yao, V. J., and Spudich, J. L. (1992) *Proc. Natl. Acad. Sci. U.S.A. 89*, 11915−11919.
12. Falke, J. J., Bass, R. B., Butler, S. L., Chervitz, S. A., and Danielson, M. A. (1997) *Annu. Rev. Cell Dev. Biol. 13*, 457−512.
13. Scherrer, P., McGinnis, K., and Bogomolni, R. A. (1987) *Proc. Natl. Acad. Sci. U.S.A. 84*, 402−406.
14. Wolff, E. K., Bogomolni, R. A., Scherrer, P., Hess, B., and Stoeckenius, W. (1986) *Proc. Natl. Acad. Sci. U.S.A. 83*, 7272−7276.
15. Spudich, E. N., Sundberg, S. A., Manor, D., and Spudich, J. L. (1986) *Proteins 1*, 239−246.
16. Spudich, J. L., and Bogomolni, R. A. (1984) *Nature 312*, 509−513.
17. Bogomolni, R. A., and Spudich, J. L. (1987) *Biophys. J. 52*, 1071−1075.
18. Szundi, I., and Bogomolni, R. A. (1996) *Biophys. J. 70*, A358.
19. Szundi, I., Lewis, J. W., and Kliger, D. S. (1997) *Biophys. J. 73*, 688−702.
20. Yan, B., and Spudich, J. L. (1991) *Photochem. Photobiol. 54*, 1023−1026.
21. Tomioka, H., Kamo, N., Takahashi, T., and Kobatake, Y. (1984) *Biochem. Biophys. Res. Commun. 123*, 989−994.
22. Haupts, U., Eisfeld, W., Stockburger, M., and Oesterhelt, D. (1994) *FEBS Lett. 356*, 25−29.

23. Spudich, J. L., Zacks, D. N., and Bogomolni, R. A. (1995) *Isr. J. Chem. 35*, 495−513.
24. Kriebel, A. N., Gillbro, T., and Wild, U. P. (1979) *Biochim. Biophys. Acta 546*, 106−120.
25. Bogomolni, R. A., Fukushima, J. G., Swartz, T., and Szundi, I. (1997) *Biophys. J. 72*, A16.
26. Spudich, E. N., and Spudich, J. L. (1993) *J. Biol. Chem. 268*, 16095−16097.
27. Bogomolni, R. A., Stoeckenius, W., Szundi, I., Perozo, E., Olson, K. D., and Spudich, J. L. (1994) *Proc. Natl. Acad. Sci. U.S.A. 91*, 10188−10192.
28. Olson, K. D., and Spudich, J. L. (1993) *Biophys. J. 65*, 2578−2585.
29. Haupts, U., Bamberg, E., and Oesterhelt, D. (1996) *EMBO J. 15*, 1834−1841.
30. Olson, K. D., Deval, P., and Spudich, J. L. (1992) *Photochem. Photobiol. 56*, 1181−1187.
31. Spudich, J. L., and Bogomolni, R. A. (1983) *Biophys. J. 43*, 243−246.
32. Rath, P., Spudich, E., Neal, D. D., Spudich, J. L., and Rothschild, K. J. (1996) *Biochemistry 35*, 6690−6696.
33. Szundi, I., and Bogomolni, R. A. (1995) *Biophys. J. 68*, A124.
34. Jung, K. H., Spudich, E. N., Dag, P., and Spudich, J. L. (1999) *Biochemistry 38*, 13270−13274.
35. Bogomolni, R. A., Stoeckenius, W., Szundi, I., Perozo, E., Olson, K. D., and Spudich, J. L. (1994) *Proc. Natl. Acad. Sci. U.S.A. 91*, 10188−10192.
36. Bogomolni, R. A., and Spudich, J. L. (1995) in *Archaea: a laboratory manual* (Robb, F. T., Ed.) pp 63−73, Cold Spring Harbor Laboratory Press, Plainview, NY.
37. Hug, S. J., Lewis, J. W., Einterz, C. M., Thorgeirsson, T. E., and Kliger, D. S. (1990) *Biochemistry 29*, 1475−1485.
38. Deleted in proof.
39. Lozier, R. H., Bogomolni, R. A., and Stoeckenius, W. (1975) *Biophys. J. 15*, 955−962.
40. Diller, R., Iannone, M., Cowen, B. R., Maiti, S., Bogomolni, R. A., and Hochstrasser, R. M. (1992) *Biochemistry 31*, 5567−5572.
41. Diller, R., Iannone, M., Bogomolni, R., and Hochstrasser, R. M. (1991) *Biophys. J. 60*, 286−289.
42. Bogomolni, R. A. (1984) in Information and energy transduction in biological membranes: Proceedings of the International Conference on Biological Membranes (Bolis, L., Helmreich, E. J. M., and Passow, H., Eds.) Crans-sur-Sierre (Valais), Switzerland, June 13−17, 1983, pp 6−12, Liss, New York.
43. Zimányi, L., Cao, Y., Chang, M., Ni, B., Needleman, R., and Lanyi, J. K. (1992) *Photochem. Photobiol. 56*, 1049−1055.
44. Tittor, J., Schweiger, U., Oesterhelt, D., and Bamberg, E. (1994) *Biophys. J. 67*, 1682−1690.
45. Turner, G. J., Miercke, L. J., Thorgeirsson, T. E., Kliger, D. S., Betlach, M. C., and Stroud, R. M. (1993) *Biochemistry 32*, 1332−1337.
46. Krebs, M. P., Spudich, E. N., and Spudich, J. L. (1995) *Protein Expression Purif. 6*, 780−788.

BI0013290